Chemistry–A European Journal

Full Paper
doi.org/10.1002/chem.202102585

**Chemistry
Europe**
European Chemical
Societies Publishing

In-Fjord Substitution in Expanded Helicenes: Effects of the Insert on the Inversion Barrier and Helical Pitch

Samuel Suárez-Pantiga,[a] Pablo Redero,[a] Xaiza Aniban,[b] Martin Simon,[a] Christopher Golz,[a] Ricardo A. Mata,*[b] and Manuel Alcarazo*[a]
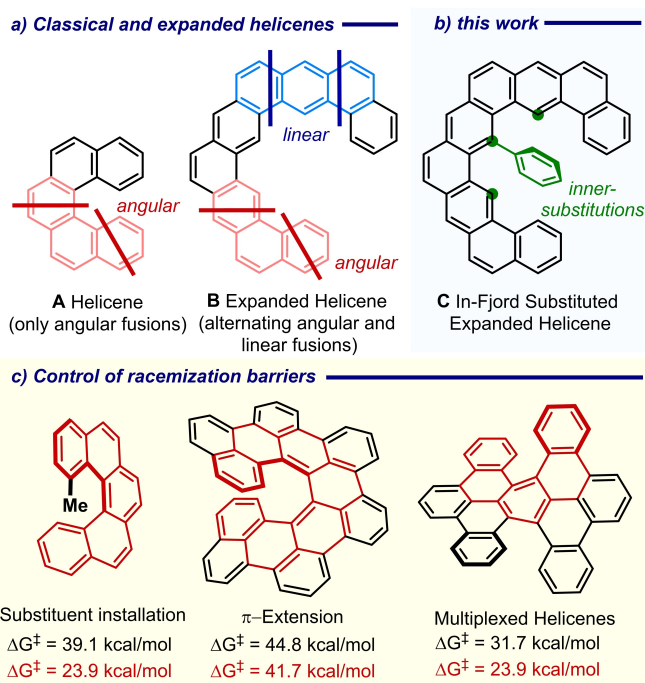
Abstract: A series of expanded helicenes of different sizes and shapes incorporating phenyl- and biphenyl-substituents at the deepest part of their fjord have been synthesized via sequential Au-catalyzed hydroarylation of appropriately designed diynes, and their racemization barriers have been calculated employing electronic structure methods. These show that the overall profile of the inversions (energies, number of transition states and intermediates, and their relative position) is intensively affected by the interplay of steric and attractive London dispersion interactions. Hence, in-fjord substitution constitutes an additional tool to handle the mechanical properties in helicenes of uncommonly large diameter. The photochemical characterization of the newly prepared helical structures is also reported.

Introduction

Classical helicene structures consists of a series of ortho-fused (hetero)aromatic rings, which on growing adopt a screw-shaped tridimensional conformation (**A**, Figure 1).[1] These compounds have been intensively studied not only for the synthetic challenges that their preparation holds, but also for the unique properties that they display in areas as remote as (asymmetric) catalysis,[2] molecular machines,[3] optoelectronic devices,[4] crystal engineering[5] or molecular recognition.[6] Recent milestones achieved in helicene synthesis comprise the thermodynamic equilibration after cyclization of diastereomeric mixtures to afford enantiopure [6]- and [7]-helicenes,[7] or the preparation of helical bilayer nanographenes[8] and multi-pole helicenes.[9]

By relaxing the condition of ortho-fusion between rings, for example allowing alternating linear and angular ring connections, expanded helicene scaffolds emerge (**B**, Figure 1). As a direct consequence of the more lax ring fusion rules, expanded helicenes invariably increase their radii and depict more torsional flexibility than "orthodox" ones. This translates into a slight reduction of their helical pitches, and much lower

[a] Dr. S. Suárez-Pantiga, P. Redero, M. Simon, Dr. C. Golz, Prof. Dr. M. Alcarazo
     Institut für Organische und Biomolekulare Chemie
     Georg-August-Universität Göttingen
     Tammannstraße 2, 37077 Göttingen (Germany)
     E-mail: malcara@gwdg.de

[b] X. Aniban, Prof. Dr. R. A. Mata
     Institut für Physikalische Chemie
     Georg-August-Universität Göttingen
     Tammannstraße 6, 37077 Göttingen (Germany)
     E-mail: rmata@gwdg.de

Figure 1. (a) Ring connectivity in helicenes and expanded helicenes; (b) Positioning in-fjord substituents in expanded helicenes; (c) Known strategies to fix the conformation in helicenes.

configurational stabilities; indeed, no configurationally stable expanded helicene that follows the alternating pattern **B** has been reported to date.[10,11]

A well-known strategy to freeze the racemization in helicenes consists of the incorporation of substituents at one or both termini of their fjord region.[12] Alternatively, higher racemization barriers are achieved by the embedment of the helicene moiety into more extended π-systems (extended helicenes),[13] or into polyhelical scaffolds (multi-pole

Chemistry–A European Journal

Full Paper
doi.org/10.1002/chem.202102585

**Chemistry
Europe**
European Chemical
Societies Publishing

helicenes);[9,14] these structures require the simultaneous deformation of several helicene units to achieve helical inversion. We hypothesized however, that an additional manifold to control inversion barriers might be operative in the case of extended helicenes. Each linear fusion incorporated to the helicene framework entails positioning a C—H moiety at their inner fjord region. Installation of suitable substituents at one or some of these in-fjord positions should increase the helical pitch of the resulting helicene and expectedly also the strain during the enantiomer interconversion process. As a result, augmented configurational stability is expected (Figure 1).

Determined to assess the viability of that working hypothesis, and as a continuation to our efforts to enable the (asymmetric) construction of helicenes and related structures,[15] we embarked on the synthesis of in-fjord-substituted expanded helicenes **C** employing phenyl and biphenyl groups as internal substituents. Given the already proven versatility of Au-catalysis to assemble complex polyaromatic architectures via alkyne hydroarylation, this transformation was chosen as the key tool for the final assembly of the desired structures.[16,17] Thus, we describe herein the synthesis of three expanded helicenes **1–3** that rigorously follow an alternation of linear/angular ring fusion pattern, and compound **4**, which is a hybrid between classical helicenes (consecutive angular fusions at both arm termini) and expanded ones (angular-linear alternation in its central section). All **1–4** derive from π-extensions of the benzo[a]phenanthro[2,3-o]pentaphene core, and bear either a phenyl or a biphenyl group at the deepest position of their internal cavity (Figure 2). The three-dimensional structures of these compounds have been determined by X-ray crystallography and their helical inversions processes evaluated with the help of state-of-the-art quantum mechanical calculations. Their photophysical characterization is reported as well.
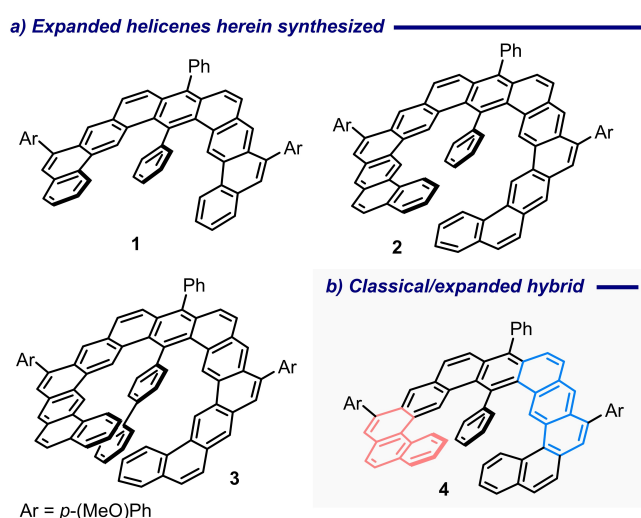
Results and Discussion

Synthesis of expanded helicenes

The route developed to prepare helicenes **1–4** starts from commercially available 2,7-napthalenediol **5**, which was effectively transformed into xanthenes **6a,b** by reaction with half equivalent of the appropriate aromatic aldehyde under acidic catalysis (Scheme 1). Subsequent triflation of both alcohols in **6a,b** was followed by oxidation of the polycyclic core with PbO$_2$, and acid-promoted elimination to afford key pyrilium salts **8a,b** in moderate yields (52% and 34%, respectively; 2 steps). Next, the desired benzo[m]tetraphene cores were obtained by condensation of **8a,b** with sodium phenylacetate in acetic anhydride followed by in situ decarboxylation. This sequence affords intermediates **9a,b** in gram scale as white solids, which can be stored for months under atmospheric conditions without apparent decomposition. Compounds with structures analogous to that of **9a,b** but having Br-substituents instead of triflates in positions 2 and 12 have been described by Müllen following an otherwise identic route.[18] We strongly recommend however the use of bistriflates **9a,b** due to their higher solubility in typical organic solvents, which facilitates their handling, purification and further transformation (Scheme 1).

Initial attempts to couple **9a** with an excess amount of boronic acid **10a'** (5.0 equiv.) via Suzuki reaction afforded **11** albeit with quite modest yield; the protodeborylation of **10a'** is the main process observed. After extensive experimentation the Negishi reaction was identified as the most efficient route to couple **9a,b** with internal alkynes **10a–c**.[19] Careful optimization of the reaction conditions (2.5 mol% Pd$_2$(dba)$_3$, 15 mol% S-Phos, 100°C (μw), 30 min.) allowed the isolation of key precursors **11–14** in 68, 91, 77 and 66% yields, respectively. The use of microwaves instead of conventional heating dramatically accel-

Figure 2. Target helicoidal structures reported in this work.
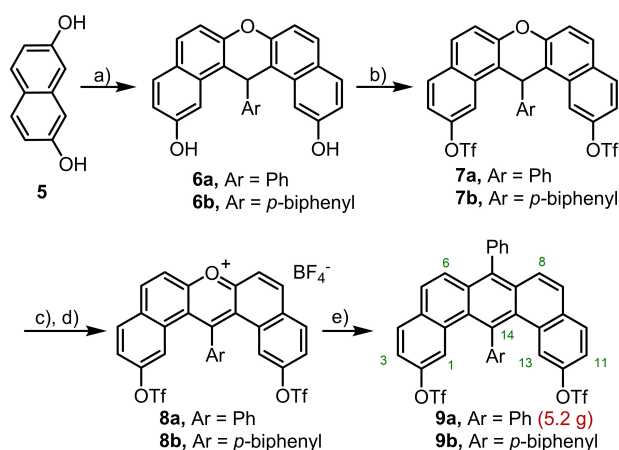
Scheme 1. Synthesis of the benzo[m]tetraphene core platform. Reagents and conditions: a) PhCHO (0.5 equiv.), p-TsOH (2 mol%), 110°C, 32 h., **6a**, 84%; **6b**, 82%; b) Tf$_2$O (2 equiv.), Et$_3$N (2 equiv.), −78°C→r.t., **7a**, 99%; **7b**, 90%; c) PbO$_2$ (3.1 equiv.), AcOH, reflux; d) HBF$_4$ (5.0 equiv.), Ac$_2$O, 0°C, **8a**, 53%; **8b**, 39% (over two steps); e) BnCO$_2$Na (1 equiv.), 150°C, Ac$_2$O, **9a**, 53%; **9b**, 16%.

Chem. Eur. J. **2021**, 27, 13358–13366   www.chemeurj.org

13359   © 2021 The Authors. Chemistry - A European Journal published by Wiley-VCH GmbH

Chemistry–A European Journal

Full Paper
doi.org/10.1002/chem.202102585

Chemistry Europe
European Chemical
Societies Publishing

erates this step of the route and even improves the yields (Scheme 2A).[20] Note that *p*-anisyl substituents were strategically located at the alkyne termini of **11–14** with the aim of suppressing parasitic 5-*exo*-dig cyclizations and the subsequent formation of non-benzenoid rings during the final twofold Au-catalyzed hydroarylation reaction.

As an additional difficulty during that last step, each of both hydroarylation events may occur at two competing sites of the benzo[*m*]tetraphene core, the electronically more activated but sterically hindered positions 1 and 13, or the more accessible external ones (positions 3 and 11). For that reason, extensive screening of reaction conditions was necessary, leading to the identification of catalyst **15** as the optimal one to assemble the desired helicene skeletons in terms of conversion and regioselectivity.[21] Under these optimized conditions, compounds **1–4** were isolated in 66%, 72%, 44% and 62% yields, respectively. (See the Supporting Information for all optimization details and also for the characterization of undesired regioisomers **16 a,b**, obtained during the process).[22]

X-ray crystallography

Single-crystals suitable for X-ray analyses of **1**, **3** and **4** were grown from slow diffusion of hexane into concentrated solutions of the title compounds in carbon disulfide, or alternatively by slow evaporation of saturated toluene solutions (See Figure 3A–C and the Supporting Information).
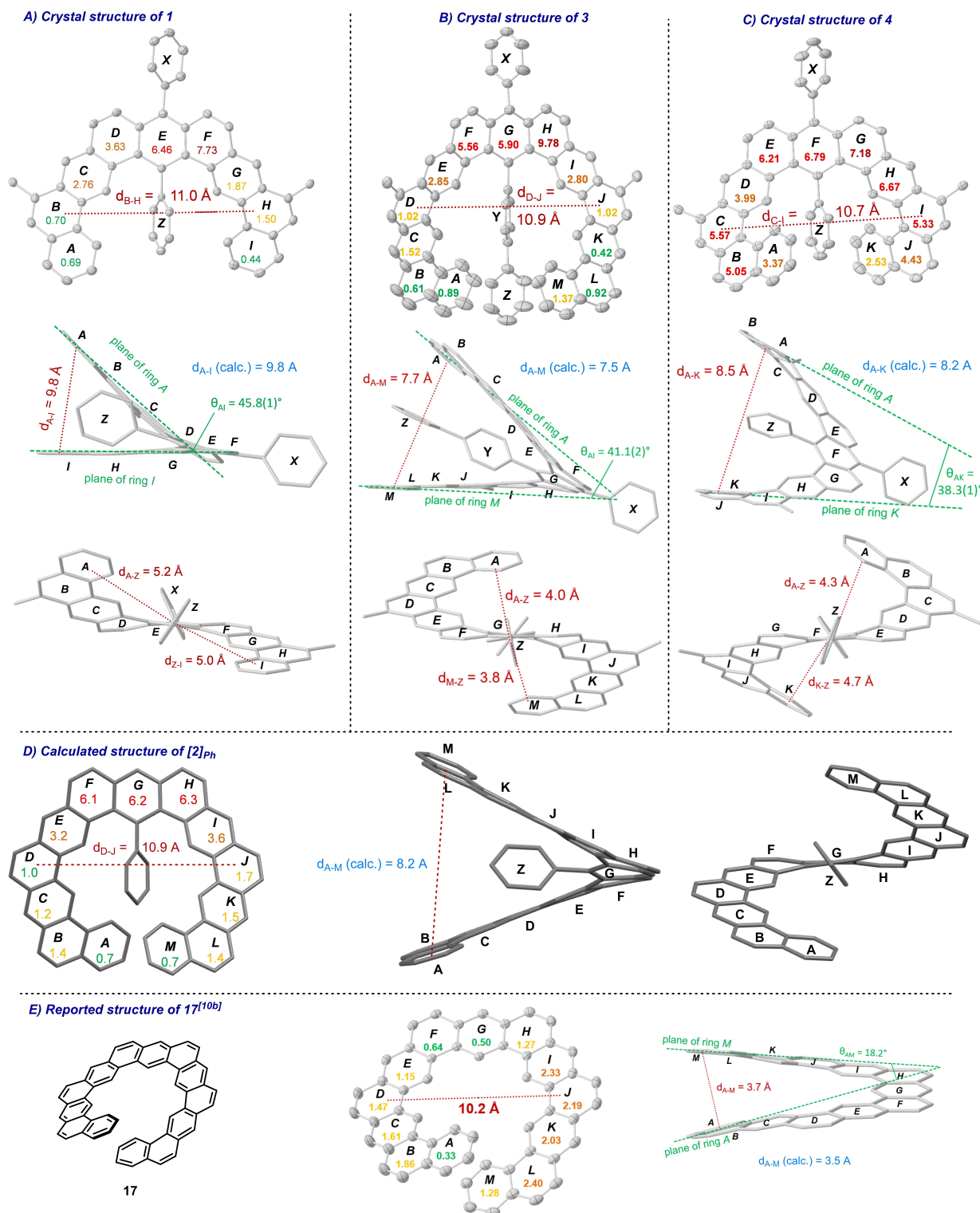
While **1** already shows a clear deviation of the planarity due to the presence of the inner Ph-group, its arms are relatively short and therefore, the comparison of the structures of **3** and **17**[10b] is the one that best portrays the influence of in-fjord substitution in the structural deformation, electronic structure, local aromaticity, and indirectly also on the helical inversion barrier of π-expanded helicenes (Figure 3). Compound **3** crystallizes as racemate (space group *R*-3); the two enantiomers separately stack along the *c*-axis, each one rotated 120° respect to its two closest neighbors, in the way that parallel columns of only *P*- and *M*-enantiomers are formed. Rings D, E and I, J of consecutively pilled molecules overlap, with a shortest π-stacking distance of 3.5 Å; disordered hexane molecules occupy the channel in between these columns.

As expected, the helical pitch of **3**, measured as the vertical distance from the centroids of the terminal A and M rings, is significantly larger than the one of **17** ($d_{A-M} = 7.7$ Å in **3**, versus $d_{A-M} = 3.7$ Å in **17**); but interestingly, the necessary distortion to accommodate the biphenyl insert does not distribute evenly along the structure as reflected from the torsion angles along the helical inner rim ($\Phi = 4.1°$, 4.0°, 14.6°, 21.3°, 1.6°, 4.5° for **3**). It accumulates in the most internal anthracene unit of the fjord cavity, rings F, G and H, while both helical arms are virtually planar. This is also evident from the comparison of the root mean square deviation (RMS) of the carbon atom positions from the mean plane of the benzene ring to which they belong. The values in % are represented inside of the rings in Figure 3.

The Y-ring of the biphenyl insert also originates repulsive interactions with the internal protons of rings E and I. This
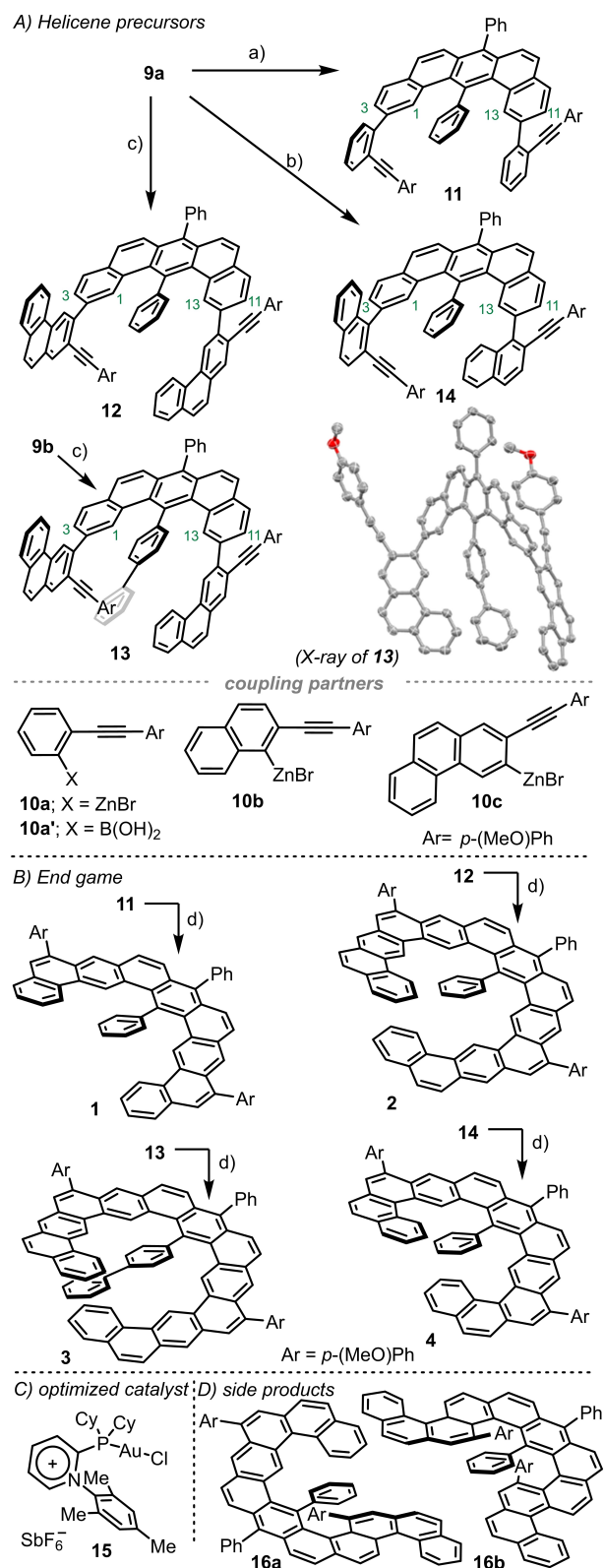
Scheme 2. (A) Synthesis of helicene precursors. Reagents and conditions: a) **10 a** (5.0 equiv.), Pd₂(dba)₃ (2.5 mol%), S-Phos (15 mol%), μw 100 °C, 68%; b) **10 b** (5.0 equiv.), otherwise as a), 91%; c) **10 c** (5.0 equiv.), otherwise as a); **12**, 77%; **13**, 66%; (B) 2-fold Au-catalyzed hydroarylation step, d) **15** (10 mol%), AgSbF₆ (10 mol%), CH₂Cl₂ or Cl₂(CH)₂Cl₂, 20 °C, **1**, 66%; **2**, 72% **3**, 44%; **4**, 62%; C) optimized Au-catalyst; D) Additional regioisomers obtained during the optimization of the reaction conditions.[23]

Chemistry–A European Journal

Full Paper
doi.org/10.1002/chem.202102585

Chemistry
Europe
European Chemical
Societies Publishing

Figure 3. A)–C) X-ray structures of **1**, **3**, **4**. Only the *ipso*-carbon from the external *p*-(MeO)Ph substituents is shown. H atoms are removed for clarity; ellipsoids are represented at 50% probability for **1** and **4**, and 15% for **3**. Root mean square deviation (RMS) from mean plane of each benzene ring given in %. D) Calculated structure of [2]$_{Ph}$ at the PBEh3c level of theory. E) Reported structure of **17**.[23]

results in an opening of the helicene arms in a plane perpendicular to the helicoidal axis, which increases the helical diameter of **3** ($d_{D-J} = 10.9$ Å) when compared with that of the unsubstituted core structure **17** ($d_{D-J} = 10.2$ Å) (Figure 3B and E). Remarkably, the terminal edges of the helicene arms in **3** (rings A and M, respectively) are conveniently stacked on the top and

Chemistry–A European Journal

Full Paper
doi.org/10.1002/chem.202102585

Chemistry Europe
European Chemical
Societies Publishing

bottom of ring Z of the biphenyl insert, respectively; being the interplanar distances, measured from the centroids of the rings, $d_{A-Z} = 4.0$ Å and $d_{M-Z} = 3.8$ Å and $d_{A-M} = 7.7$ Å. These values are very similar to the pitches found in high order helicenes such as for example [*16*]helicene.[24] Although we were not able to obtain the X-ray structure of **2** our calculations, which closely reproduce the pitches of **1**, **3** and **4**, predict a $d_{A-M} = 8.2$ Å in that architecture. This counterintuitive result, which implies a longer helical pitch for **2** than for **3**, can only be explained by presuming the presence of attractive π-π interactions between the helicene arms and ring Z of the insert in **3** (See the computational section and the Supporting Information).

The solid-state structure of **4** is quite informative as well. The molecule adopts an approximately C_2-symmetric conformation, and its helical pitch measured from the centroids of the rings A, and K (8.5 Å) is the biggest one in the series due to the angular-angular junction of terminal rings A–B and J–K, which increases the unfavorable steric interaction of these moieties with ring Z and forces ring tilting also at the arms. As a result, the torsion angles along the helical inner rim ($\Phi = 20.4°$, 20.0°, 20.4°, 25.7°, 21.5°, 17.5°) and the RMS deviation of the carbon atoms from the ideal benzene plane reveal evenly distributed deformations along with the complete structure. This distinguishes **4** from **1** ($\Phi = 1.1°$, 14.9°, 25.7°, 6.2°) and **3** (Figure 3A–C). None of the structures synthesized is configurationally stable at room temperature.

Electronic structure calculations and helical inversion mechanism

Having developed an efficient synthesis for **1**–**4**, we examined their conformational dynamics by Density Functional Theory (DFT) calculations. In order to obtain specific insight about the influence of the inner substitution in the inversion barrier heights, the pathways were calculated not only for compounds **1**–**4**, but also we included the unsubstituted core architectures. All structures were optimized at the PBEh3c level of theory,[25] with energies recomputed with the double hybrid functional B2PLYP,[26] including D3 dispersion corrections with Becke-Johnson damping,[27] the def2-TZVP basis set[28] and default fitting basis.[29] Nudged elastic band calculations (NEB) were carried out to obtain a conversion profile, with energy estimates for the barrier provided by the climbing image. In cases where the conversion mechanism crosses a *Cs*-symmetric intermediate, the energy profiles were only computed for one stretch of the pathway and then symmetrized. The aforementioned calculations were carried out with the Orca 4.2.1 program package.[30] All substitutions in the outer rim were removed to minimize computation time. These structures are represented by the number of the real ones in parenthesis; the internal substituent is indicated as subindex. The energies reported are electronic energies unless otherwise noted. The difference between the latter values and Gibbs free energy barriers are small. In order to better understand some of the trends observed, we have carried out dispersion interaction density (DID) analyses of the structures.[31] The energies were computed
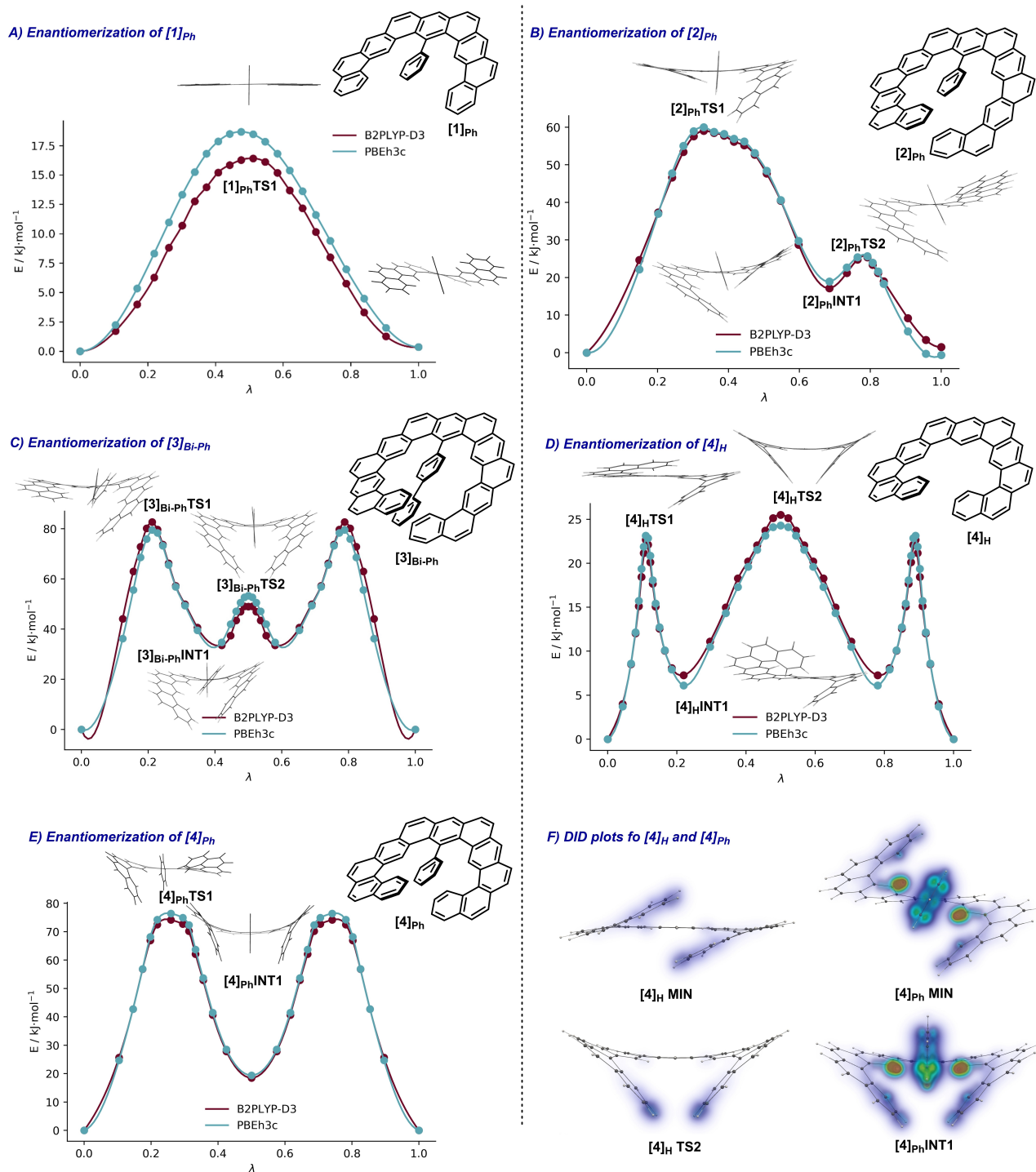
at the SCS-LMP2 level of theory with the Molpro2020.1 program package.[32,33] Details for the calculation setup, in particular how the intramolecular analysis was defined, are provided in Supporting Information.

In the case of unsubstituted **1**, i.e. [**1**]$_H$, no helix is formed, and the most stable structure adopts a planar conformation, as expected. Upon introduction of the phenyl substituent, two enantiomeric conformations of compound [**1**]$_{Ph}$ become apparent, yet separated by a single and rather small barrier [**1**]$_{Ph}$**TS1** of only 15.9 kJ·mol⁻¹ in the NEB computed energy profile (free barrier for activation of 19.1 kJ·mol⁻¹, Figure 4A). More interesting, however, are the cases of compounds **2**–**4**. Their potential energy hypersurfaces are more complex, and in all cases the interconversions take place via stepwise mechanisms (shown in Figure 4B–E).

The energetic profile for the racemization of [**2**]$_{Ph}$ is shown in Figure 4. The barrier has been calculated to be $\Delta E^{\ddagger} = 59.0$ kJ·mol⁻¹, which is very similar to the one reported for the unsubstituted **17** ($\Delta G^{\ddagger} = 54.3$). This indicates that the presence of the phenyl insert in **2** does not significantly modify the height of its inversion barrier, probably due to the length of the arms. However, and exceptionally along the series, the potential energy diagram of [**2**]$_{Ph}$ is not C_s symmetric, implying that through the minimum energy pathway both arms move coordinated but at different paces. Thus, while the left one in Figure 4B nearly achieves the central anthracene plane, the right one squirms itself to facilitate this step [**2**]$_{Ph}$**TS1**. Once the left arm achieves its final position [**2**]$_{Ph}$**INT1**, the right one proceeds to complete the enantiomerization, now via a quite low barrier [**2**]$_{Ph}$**TS2**, since it is already appropriately positioned. This avoids the C_s structure which would be even higher in energy due to the steric clash between the phenyl substituent and the arms.

The formal exchange of the phenyl insert by a biphenyl one delivers [**3**]$_{Bi-Ph}$. At first glance, our calculations indicate that an additional penalty of around 20 kJ·mol⁻¹ needs to be satisfied for the inversion to take place ($\Delta E^{\ddagger} = 82.7$ kJ·mol⁻¹). This can be attributed to two factors: the loss of the stabilizing π-stacking interaction between the Z-ring of the biphenyl and the arm that starts the inversion, and the need to bend away the internal substituent more abruptly than in [**2**]$_{Ph}$ to reduce steric hindrance. More striking is that the potential energy diagram is again C_s symmetric, suggesting that both arms operate independently, one after the other. In addition, the C_s-symmetric conformer corresponds to a local energetic maximum, [**3**]$_{Bi-Ph}$**TS2**; slight rotation of the biphenyl Z ring either to the right or the left reestablish a stabilizing π-staking interaction with one or the other arm [**3**]$_{Bi-Ph}$**INT1** (Figure 4C).

In order to understand the behavior of the more rigid **4**, the inversion process in structures [**4**]$_H$ and [**4**]$_{Ph}$ were studied as well (Figure 4D–E). In [**4**]$_H$ one of the [4]helicene moieties located at the end of the arms initially inverts via [**4**]$_H$**TS1** to form an intermediate [**4**]$_H$**INT1**, whereby the inverting arm edge ring points towards the opposing arm. From this point, the C_s symmetric [**4**]$_H$**TS2** transition state is found, exhibiting a rather similar barrier. This structure shows the two arms pointing in the same direction. A completely symmetric process involving

Chemistry–A European Journal

Full Paper
doi.org/10.1002/chem.202102585

Chemistry
Europe
European Chemical
Societies Publishing

Figure 4. NEB energy profiles for the enantiomerization mechanisms of: A) [1]$_{Ph}$, B) [2]$_{Ph}$, C) [3]$_{Bi-Ph}$, D) [4]$_H$, and E) [4]$_{Ph}$ calculated at the PBEh3c level of theory (single point calculations at the B2LYP-D3/def2-TZVP level). The independent coordinate λ is the normalized abelian distance between atoms from reactant to transition state. Only selected transition states and energy-minimum structures are represented together to the energy profiles.; f) DIDs for the interactions between the arms and the central substituent in [4]$_{Ph}$ calculated at the SCS-LMP2 level.

the other arm furnishes *ent*-[4]$_H$. The barrier to helical inversion for this process was calculated to be $\Delta E^{\ddagger} = 25.5$ kJ·mol^{-1} corresponding to the barrier in [4]$_H$TS2. Saving the distances in terms of absolute energy values, the shape of the isomerization

profile and the inversion mechanism in [4]$_H$ is very similar to that described for [8]helicene.[34]

Introduction of the internal Ph-substituent in [4]$_{Ph}$ substantially changes the shape of the isomerization profile. Instead of three transition states, only two symmetrical relatively high

Chemistry–A European Journal

Full Paper
doi.org/10.1002/chem.202102585

Chemistry Europe
European Chemical
Societies Publishing

barriers ($\Delta E^{\ddagger} = 74.2$ kJ·mol^{-1}) are observed. The transition states are similar in structure to **[4]$_H$TS1** (inversion of a terminal [4] helicene moiety), but the C_s-symmetric structure with the two arms facing each other is no longer the highest transition state as in **[4]$_H$**. Instead, it is a minimum, **[4]INT1**. This might seem counterintuitive at first, since the Ph-substituent should always contribute to the steric strain, imposing more pronounced deformations to the helical framework; however, a closer look reveals that this is an incomplete analysis. First, the Ph-substituent adds foremost a penalty when one arm points towards the center of the helix. If we compare the barriers between **[4]$_H$TS1** and **[4]$_{Ph}$TS1** (22.7 vs. 74.2 kJ·mol^{-1}), which is a fair comparison given the similarity between the structures, the difference is 51.5 kJ·mol^{-1}. This is a first approximation to the added penalty as the result of the augmented steric clash in **[4]$_{Ph}$**. However, in the C_s-symmetric structure, the Ph-substituent actually acts as a slightly stabilizing factor. The **[4]$_{Ph}$INT1** structure is 18.5 kJ·mol^{-1} above the global minimum, while the same structural motif in **[4]$_H$**, which is actually a transition state, is 25.5 kJ·mol^{-1} above the starting configuration. Attractive London dispersion forces, which are now operative between the final edges of the arms and the middle phenyl group, account for this fact. We have plotted in Figure 4F the dispersion interaction densities (DIDs) for the interactions between the arms and the central substituent in **[4]$_{Ph}$** and compared them (using the same scale) to the interactions between the arms in the case of **[4]$_H$**. The dispersion interactions (quantified at the SCS-LMP2 level) show a stark contrast. In **[4]$_{Ph}$INT1** they amount to 29 kJ·mol^{-1}, with the value going down to just 3 kJ·mol^{-1} in the case of **[4]$_H$TS2**. Hence, we conclude that the London forces derived from the presence of the Ph-insert effectively compensate the energetic penalty to be paid in **[4]$_{Ph}$INT1** due to the more pronounced deformation of the polyaromatic skeleton. From this analysis we concluded that the inversion barrier in **[4]$_{Ph}$** is probably lowered by dispersion as well since this interaction is also present, at least in part, in **[4]$_{Ph}$INT1** between the Ph-insert and one of the helicene arms.

None of the barriers calculated is sufficiently high to allow the resolution of the enantiomers of **1–4** at room temperature. However, these examples do show how the inversion pathway of the original helicene scaffold can be modified upon substitution; even by eliminating or creating new barriers to surmount. In general, the steric impact of the in-fjord substitution increases racemization barriers, but this effect cannot be simply correlated with the size of the substituent.

UV-Vis absorption and emission

The UV absorption and emission spectra of **1–4** and **16 a,b** have been measured in chloroform at room temperature (absorption) and 10 °C (emission); those for **1–4** are summarized in Figure 5. Table 1 contains all relevant numerical data.

Three sets of comparable absorption bands can be identified in the UV-Vis spectra of **1–4** in the 280–340, 360–400 and 380–420 nm regions. As expected, the spectra for **2–3** are quite
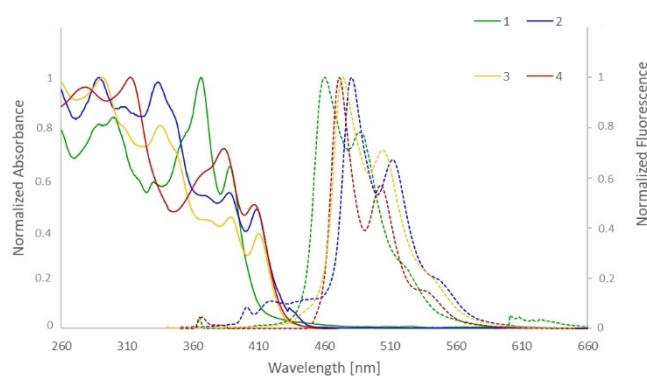

Figure 5. (a) Normalized UV-Vis absorption (continuous line) and fluorescence spectra (dotted line) of **1–4** in HCCl$_3$ at room temperature.

Table 1. Photophysical properties.[a]

Compound	Absorption λ_{max} (nm)	ε_{max} (M^{-1}cm^{-1})	λ_{em} (nm)	Φ_f (nm)[b]
1	300	3.26×10^4	457	0.29 (366)
	366	3.88×10^4	490	
	388	2.51×10^4		
2	290	1.62×10^5	479	0.07 (333)
	333	1.59×10^5	515	
	388	8.78×10^4		
	409	7.69×10^4		
3	293	1.31×10^5	472	0.02 (330)
	336	1.09×10^5	506	
	390	6.15×10^4		
	411	5.27×10^4		
4	312	7.66×10^4	471	0.09 (312)
	383	5.49×10^4	508	
	406	3.79×10^4		
16 a	310	3.40×10^5	494	0.33 (310)
	339	2.60×10^5	521	
	390	2.70×10^5		
16 b	292	1.66×10^5	506	0.12 (321)
	321	1.68×10^5	533	
	370	1.17×10^5		
	394	1.27×10^5		

[a] Measured in HCCl$_3$ at 25 °C; [b] Excitation wavelength.

similar, but they appear bathochromically shifted compared with that of **1**; this is a consequence of the increased π-extension in these structures. Comparison of the absorption maxima of **2** and **3** with the same bands reported by **17**: 320 nm ($\varepsilon = 1.4 \times 10^5$ M^{-1}cm^{-1}), 375 nm ($\varepsilon = 3.5 \times 10^4$ M^{-1}cm^{-1}) and 395 nm ($\varepsilon = 3.8 \times 10^4$ M^{-1}cm^{-1}), also indicates a red shift of the transitions of **2** and **3** by approximately 1220 and 1490 cm^{-1}, respectively.

The fluorescence spectra follow a tendency that is consistent with the absorption spectra. The maxima for **2–4** also appear red shifted when compared to **1** ($\lambda_{em,max} = 457, 479, 472$ and 471 nm. for **1–4**, respectively).

DFT calculations have also been carried out to obtain the spectra of compounds **1–3** (see the Supporting Information). We have made use of the simplified time dependent density functional theory formalism (sTD-DFT)[35] with the ωB97X functional[36] and the def2-TZVP basis set. The functional was chosen for its correct long-range asymptotic exchange, which is

Chemistry–A European Journal

Full Paper
doi.org/10.1002/chem.202102585

Chemistry
Europe
European Chemical
Societies Publishing

important in such extended systems. Following the same procedure as in previous absorption studies for helicenes, the computed absorption energies were shifted by 1 eV.[37] The trends observed in the measured spectra are well replicated in the DFT spectra (based on PBEh3c structures). The red shifts of the transitions of **2** and **3** if compared to **17** can be traced back to their increased helical pitches. A comparison between computed and experimental absorption spectra is provided in the Supporting Information.

Conclusion

In summary, we describe herein the design and synthesis of expanded helicenes containing substituents attached to the inner part of their cavity. Key for the preparation of these unique architectures was the identification of a highly reactive Au-catalyst, **15**, which allows the key hydroarylation steps to proceed not only efficiently in terms of yield, but also with high regioselectivity. Comparison of the enantiomerization energy profile of the targeted helicenes with these of their unsubstituted parent structures show significant differences in the relative energy values and in the general shape of the profile (number of transition states and intermediates). These changes cannot be simply correlated with the size of the insert. Hence, our results demonstrate that deep in-fjord substitution can be used as an additional tool to handle the mechanical properties of expanded helicenes. Moreover, they also highlight the impact of dispersion interactions in the enantiomerization of these architectures, and how they may counteract the expected tendencies from the classical concept of steric hindrance.

Conflict of Interest

The authors declare no conflict of interest.

Keywords: expanded helicenes · Au catalysis · hydroarylation · polycyclic aromatic compounds · racemization barriers

[1] a) Y. Shen, C. F. Chen, *Chem. Rev.* **2012**, *112*, 1463–1535; b) M. Gringas, G. Félix, R. Peresutti, *Chem. Soc. Rev.* **2013**, *42*, 1007–1050; c) M. Gringas, *Chem. Soc. Rev.* **2013**, *42*, 1051–1095; d) T. Mori, *Chem. Rev.* **2021**, *121*, 2372–2412.

[2] a) K. Yavari, P. Aillard, Y. Zhang, F. Nuter, P. Retailleau, A. Voituriez, A. Marinetti, *Angew. Chem. Int. Ed.* **2014**, *53*, 861–865; b) P. Aillard, A. Voituriez, A. Marinetti, *Dalton Trans.* **2014**, *43*, 15263–15278.

[3] S. Kassem, T. van Leeuwen, A. S. Lubbe, M. R. Wilson, B. L. Feringa, D. A. Leigh, *Chem. Soc. Rev.* **2017**, *46*, 2592–2621.

[4] a) T. J. Wigglesworth, D. Sud, T. B. Norsten, V. S. Lekhi, N. R. Branda, *J. Am. Chem. Soc.* **2005**, *127*, 7272–7273; b) N. Islam, A. H. Pandit, *J. Mol. Model.* **2014**, *20*, 2535; c) W.-L. Zhao, M. Li, H.-Y. Lu, C.-F. Chen, *Chem. Commun.* **2019**, *55*, 13793–13803; d) M. Milton, N. J. Schuster, D. W. Paley, R. Hernández Sánchez, F. Ng, M. L. Steigerwald, C. Nuckolls, *Chem. Sci.* **2019**, *10*, 1029–1034.

[5] a) M. Tounsi, M. Ben Braiek, H. Barhoumi, A. Baraket, M. Lee, N. Zine, A. Maaref, A. Errachid, *Mater. Sci. Eng. C* **2016**, *61*, 608–615; b) T. Fujikawa, N. Mitoma, A. Wakamiya, A. Saeki, Y. Segawa, K. Itami, *Org. Biomol. Chem.* **2017**, *15*, 4697–4703.

[6] a) L. Fang, M. Li, W.-B. Lin, Y. Shen, C.-F. Chen, *J. Org. Chem.* **2017**, *82*, 7402–7409; b) A. Mairena, J. I. Mendieta, O. Stetsovych, A. Terfort, I. G. Stará, I. Starý, P. Jelínek, K. H. Ernst, *Chem. Commun.* **2019**, *55*, 10595–10598.

[7] M. Šámal, S. Chercheja, J. Rybáček, J. V. Chocholoušová, J. Vacek, L. Bednárová, D. Šaman, I. G. Stará, I. Starý, *J. Am. Chem. Soc.* **2015**, *137*, 8469–8474.

[8] a) P. J. Evans, J. Ouyang, L. Favereau, J. Crassous, I. Fernández, J. Perles, N. Martín, *Angew. Chem. Int. Ed.* **2018**, *57*, 6774–6779; b) M.-G. Rong, J. Wang, J. Liu, *Chem. Asian J.* **2021**, *16*, 1216–1220.

[9] For selected examples see: a) T. Fujikawa, Y. Segawa, K. Itami, *J. Am. Chem. Soc.* **2015**, *137*, 7763–7768; b) X.-Y. Wang, X.-C. Wang, A. Narita, M. Wagner, X.-Y. Cao, X. Feng, K. Müllen, *J. Am. Chem. Soc.* **2016**, *138*, 12783–12786; c) Y. Hu, X.-Y. Wang, P.-X. Peng, X.-C. Wang, X.-Y. Cao, X. Feng, K. Müllen, A. Narita, *Angew. Chem. Int. Ed.* **2017**, *56*, 3374–3378; d) T. Hisokawa, Y. Takahashi, T. Matsushima, S. Watanabe, S. Kikkawa, I. Azumaya, A. Tsurusaki, K. Kamikawa, *J. Am. Chem. Soc.* **2017**, *139*, 18512–18521; e) V. Berezhnaia, M. Roy, N. Vanthuyne, M. Villa, J.-V. Naubron, J. Rodríguez, Y. Coquerel, M. Gingras, *J. Am. Chem. Soc.* **2017**, *139*, 18508–18511; f) K. Kato, Y. Segawa, L. T. Scott, K. Itami, *Angew. Chem. Int. Ed.* **2018**, *57*, 1337–1341; g) M. Roy, V. Berezhnaia, M. Villa, N. Vanthuyne, M. Giorgi, J.-V. Naubron, S. Poyer, V. Monnier, L. Charles, Y. Carissan, D. Hagebaum-Reignier, J. Rodríguez, M. Gingras, Y. Coquerel, *Angew. Chem. Int. Ed.* **2020**, *59*, 3264–3271; h) B. Liu, M. Böckmann, W. jiang, N. L. Doltsinis, Z. Wang, *J. Am. Chem. Soc.* **2020**, *142*, 7092–7099; i) A. Yubuta, T. Hosokawa, M. Gon, K. Tanaka, Y. Chujo, A. Tsurusaki, K. Kamikawa, *J. Am. Chem. Soc.* **2020**, *142*, 10025–10033.

[10] a) G. R. Kiel, S. C. Patel, P. W. Smith, D. S. Levine, T. D. Tilley, *J. Am. Chem. Soc.* **2017**, *139*, 18456–18459; b) Y. Nakakuki, T. Hirose, K. Matsuda, *J. Am. Chem. Soc.* **2018**, *140*, 15461–15469; c) G. R. Kiel, K. L. Bay, A. E. Samkian, N. J. Schuster, J. B. Lin, R. C. Handford, C. Nuckolls, K. N. Houk, T. D. Tilley, *J. Am. Chem. Soc.* **2020**, *142*, 11084–11091; d) F. Chen, W. Gu, A. Saeki, M. Melle-Franco, A. Mateo-Alonso, *Org. Lett.* **2020**, *22*, 3706–3711.

[11] Configurationally stable expanded helicenes that follow an angular-angular-linear fusion pattern are known: a) K. Fujise, E. Tsurumaki, G. Fukuhara, N. Hara, Y. Imai, S. Toyota, *Chem. Asian J.* **2020**, *15*, 2456–2461; b) K. Fujise, E. Tsurumaki, K. Wakamatsu, S. Toyota, *Chem. Eur. J.* **2021**, *27*, 4548–4552.

[12] P. Ravat, R. Hinkelmann, D. Steinebrunner, A. Prescimone, I. Bodoky, M. Juríček, *Org. Lett.* **2017**, *19*, 3707–3710.

[13] a) Y. Nakakuki, T. Hirose, H. Sotome, H. Miyasaka, K. Matsuda, *J. Am. Chem. Soc.* **2018**, *140*, 4317–4326; b) M. A. Medel, R. Tapia, V. Blanco, D. Miguel, S. P. Morcillo, A. G. Campaña, *Angew. Chem. Int. Ed.* **2021**, *60*, 6094–6100.

[14] H. Marom, S. Pogodin, I. Agranat, *Polycyclic Aromat. Compd.* **2007**, *27*, 295–310.

[15] a) E. González-Fernández, L. D. M. Nicholls, L. D. Schaaf, C. Farès, C. W. Lehmann, M. Alcarazo, *J. Am. Chem. Soc.* **2017**, *139*, 1428–1431; b) L. D. M. Nicholls, M. Marx, T. Hartung, E. González-Fernández, C. Golz, M. Alcarazo, *ACS Catal.* **2018**, *8*, 6079–6085; c) T. Hartung, R. Machleid, M. Simon, C. Golz, M. Alcarazo, *Angew. Chem. Int. Ed.* **2020**, *59*, 5660–5664; d) P. Redero, T. Hartung, J. Zhang, L. D. M. Nicholls, G. Zichen, M. Simon, C. Golz, L. M. Wolf, M. Alcarazo, *Angew. Chem. Int. Ed.* **2020**, *59*, 23527–23531.

[16] For seminal work in this transformation see: a) V. Mamane, A. Fürstner, *J. Org. Chem.* **2002**, *67*, 6264–6267; b) V. Mamane, P. Hannen, A. Fürstner, *Chem. Eur. J.* **2004**, *10*, 4556–4575.

[17] See references 11, 15 and: a) K. Nakamura, S. Furumi, M. Takeuchi, T. Shibuya, K. Tanaka, *J. Am. Chem. Soc.* **2014**, *136*, 5555–5558; b) M. Tanaka, Y. Shibata, K. Nakamura, K. Teraoka, H. Uekusa, K. Nakazono, T. Takata, K. Tanaka, *Chem. Eur. J.* **2016**, *22*, 9537–9541; c) M. Satoh, Y. Shibata, K. Tanaka, *Chem. Eur. J.* **2018**, *24*, 5434–5438.

[18] W. Zhang, Z. Chen, B. Yang, X.-Y. Wang, R. Berger, A. Narita, G. B. Barin, P. Ruffieux, R. Fasel, X. Feng, H. J. Räder, K. Müllen, *Anal. Chem.* **2017**, *89*, 14, 7485–7492.

[19] J. E. Milne, S. L. Buchwald, *J. Am. Chem. Soc.* **2004**, *126*, 13028–13032.

[20] a) P. Walla, C. O. Kappe, *Chem. Commun.* **2004**, 564–565; b) M. Genov, A. Almorín, P. Espinet, *Tetrahedron: Asymmetry.* **2007**, *18*, 625–627.

[21] H. Tinnermann, L. D. M. Nicholls, T. Johannsen, C. Wille, C. Golz, R. Goddard, M. Alcarazo, *ACS Catal.* **2018**, *8*, 10457–10463.

[22] **16a** and **16b** are configurationally stable at r.t. For the synthesis of structurally related compounds see: R. Yamano, Y. Shibata, K. Tanaka, *Chem. Eur. J.* **2018**, *24*, 6364–6370.

[23] Deposition Numbers 2062473 (**1**), 2010181 (**3**), 2062474 (**4**), 2062475 (**13**), 2062476 (**16a**), and 2062477 (**16b**) contain the supplementary crystallographic data for this paper. These data are provided free of charge by the joint Cambridge Crystallographic Data Centre and Fachinformationszentrum Karlsruhe Access Structures service.

[24] K. Mori, T. Murase, M. Fujita, *Angew. Chem. Int. Ed.* **2015**, *54*, 6847–6851.

[25] S. Grimme, J. G. Brandenburg, C. Bannwarth, A. Hansen, *J. Chem. Phys.* **2015**, *143*, 054107.

[26] S. Grimme, *J. Chem. Phys.* **2006**, *124*, 034108.

[27] a) S. Grimme, S. Ehrlich, L. Goerigk, *J. Comb. Chem.* **2011**, *32*, 1456–1465; b) S. Grimme, J. Antony, S. Ehrlich, H. Krieg, *J. Chem. Phys.* **2010** *132*, 154104.

[28] F. Weigend, R. Ahlrichs, *Phys. Chem. Chem. Phys.* **2005**, *7*, 3297–3305.

[29] a) F. Weigend, *Phys. Chem. Chem. Phys.* **2006**, *8*, 1057–1065; b) A. Hellweg, C. Hättig, S. Höfener, *Theor. Chem. Acc.* **2007**, *117*, 587–597.

[30] F. Neese, *Comp. Mol. Sci.* **2012**, *2*, 73–78.

[31] A. Wuttke, R. A. Mata, *J. Comb. Chem.* **2017**, *38*, 15–23.

[32] a) S. Grimme, *J. Chem. Phys.* **2003**, *118*, 9095; b) M. Andrejića, R. A. Mata, *Phys. Chem. Chem. Phys.* **2013**,*15*, 18115–18122.

[33] H.-J. Werner, P. J. Knowles, G. Knizia, F. R. Manby, M. Schütz, *Comp. Mol. Sci.* **2012**, *2*, 242–253.

[34] J. Barroso, J. L. Cabellos, S. Pan, F. Murillo, X. Zarate, M. A. Fernández-Herrera, G. Merino, *Chem. Commun.* **2018**, *54*, 188–191.

[35] C. Bannwarth, S. Grimme, *Comp. Theor. Chem.* **2014**, *1040–1041*, 45–53.

[36] J.-D. Chaia, M. Head-Gordon, *J. Chem. Phys.* **2008**, *128*, 084106.

[37] C. Bannwarth, J. Seibert, S. Grimme, *Chirality* **2016**, *28*, 365–369.